

A new perspective on the analysis of helix-helix  
packing preferences in globular proteins

A. Trovato and F. Seno

INFN-Dipartimento di Fisica 'G. Galilei', Università di Padova,

Via Marzolo 8, 35131 Padova, Italy

November 3, 2018

## Abstract

For many years it had been believed that steric compatibility of helix interfaces could be the source of the observed preference for particular angles between neighbouring helices as emerging from statistical analysis of protein databanks. Several elegant models describing how side chains on helices can interdigitate without steric clashes were able to account quite reasonably for the observed distributions. However, it was later recognized (Bowie, 1997 and Walther, 1998) that the “bare” measured angle distribution should be corrected to avoid statistical bias. Disappointingly, the rescaled distributions dramatically lost their similarity with theoretical predictions casting many doubts on the validity of the geometrical assumptions and models. In this report we elucidate a few points concerning the proper choice of the random reference distribution. In particular we show the existence of crucial corrections due to the correct implementation of the approach used to discriminate whether two helices are in contact or not and to measure their relative orientations. By using this new rescaling, the “true” packing angle preferences are well described, even more than with the original “bare” distribution, by regular packing models.

## Introduction

The issue of the pairwise packing between helices in proteins was addressed soon after helical structures had been suggested. A number of models were developed, mostly devoted to surface complementarities upon packing. The “knobs into holes” model, first introduced by Crick [1] and elaborated by Richmond and Richards [2], aimed to find the best steric fit between regular helices. Chothia, Levitt and Richardson [3, 4] recognized the importance of “ridges” and “grooves” formed by residues with different sequential distances (“ridges into grooves” model). Efimov [5] tried to relate the packing angle between the two helices with the preferred rotational states of the side-chains along them. A comprehensive analysis was eventually carried out by Walther et. al. [6], by modeling helix packing as the superposition of the two regular lattices that result from unrolling the helix cylinders onto a plane and contain points representing each residue. The six “preferred” angles predicted by this last model are consistent with earlier results and with the histograms of the experimentally observed packing angles (see Fig. 7 of Ref. [6]). The agreement between theoretical modeling and experimental data was remarkable, although not perfect (see Ref. [6] for a more detailed discussion).

The success of steric models in providing an explanation for the most prevalent packing angles was however put under discussion after the observation made by Bowie [7] that statistical corrections must be applied to the values collected from experimentally determined structures before true interaxial angle preferences can be revealed.

Indeed, the helix-helix packing is defined to occur only when:

- [C1] the segment of closest approach (SCA), of length  $d_R$ , between the two finite helix axes is shorter than a prefixed threshold  $d_c$ ;
- [C2] this segment intersects both helix axes at a perpendicular angle.

In Ref. [6], two helices were considered to be in contact if they were satisfying both conditions  $C1$  and  $C2$ . Note that Walther *et al.* [6] selected interacting helical pairs from their database of native protein conformations, by considering distances between all possible inter-helical heavy atom pairs. We used a different selection procedure involving distances between inter-helical  $C_\alpha$  atom pairs (see Methods for details). None of these particular choices really affects our geometrical analysis, and condition  $C1$ , as defined above, is just the simplest way of defining an equivalent distance constraint.

Condition  $C2$  is needed to ensure face-to-face packing of the two helices, justifying thus the use of theoretical modeling based on the steric interdigitation of the helices.

If the SCA is coincident with the global segment of closest approach (GSCA), of length  $d$ , between the two straight lines which are obtained by indefinitely prolonging the helix axes, condition  $C2$  is then automatically satisfied. In such a situation, which corresponds to effectively dealing with helices of infinite length (see Fig. 1a), the reference probability distribution of interaxial angles  $P(\Omega)$  is simply the spherical-polar distribution between any two random vectors, namely  $P(\Omega) \sim \sin \Omega$  [7].

Walther and co-workers [8] realized that the finiteness of helix axes is crucial in modifying the angular dependence of  $P(\Omega)$ , because requiring that the SCA intersects both axes at a perpendicular angle introduces new restrictions depending on the packing angle  $\Omega$ . This can be understood by looking at Fig. 2a, where it is shown that, fixing one helix position, and assuming the GSCA to be orthogonal to the page, the second finite helix axis may then be placed only within a plane parallel to the paper plane and such that its starting point lies inside the dark shaded parallelogram  $A$ .

The probability of placing the starting point of the second helix in  $A$  is proportional to its area and therefore to  $\sin \Omega$ . Consequently the probability  $P(\Omega)$  for selecting a particular packing angle is proportional to the product of the spherical-polar contribution and of the  $\sin \Omega$  effect due to the finite length condition:

$$P(\Omega) \sim \sin^2 \Omega \tag{1}$$

With this new random reference distribution the actual angular propensities need to be reconsidered. As is clear from Fig. 2 of Ref. [8], the normalized frequencies reveal a prominent representation of packing angles near  $0^\circ$  and  $180^\circ$  (not expected by theoretical models) whereas the predicted optimal steric packing angles manifest themselves, at most as shoulders in the distribution of propensities. The predictivity of geometrical models is cast under serious doubts after this analysis.

Our first observation is that the random distribution  $P(\Omega) \sim \sin^2 \Omega$  is correct only

and only if the condition of mutual perpendicularity between the SCA and the two axes is strictly fulfilled. But is this the real situation when statistical histograms are derived?

As a matter of fact, condition *C2* was relaxed by Walther *et al.*, by admitting a small tolerance: a total deviation  $\tau = \tau_1 + \tau_2$  ( $\tau_1$  and  $\tau_2$  are the complementary angles to the angles  $\theta_1$  and  $\theta_2$  formed between the SCA and helix 1 and helix 2, respectively (see Fig. 1b)) was accepted up to a threshold  $\tau_{\max}$  ( $\tau_{\max} = 5^\circ$  in [6] and  $\tau_{\max} = 1^\circ$  in [8]).

At first, one might wonder why such a threshold needs to be used since it does not effectively increase the number of data contributing to the histograms. However, we believe that this choice is indeed necessary because of the ambiguity in the definition of the axis direction in natural helices, which introduces an intrinsic uncertainty in the computation of the  $\Omega, \theta, \tau$  angles (see Methods for a detailed explanation of how the axis is reconstructed in the typical case of a non-ideal bent helix and for an estimation of such uncertainty  $\overline{\Delta\Omega}$ ). A relaxation of condition *C2* is thus crucial, if we want to analyse correctly data extracted from the database of real native protein structures.

We will show in this paper, by means of partly semi-analytical geometrical arguments and eventually numerical simulations, that such threshold effect does drastically change the random reference distribution. Having measured helix-helix packing angles from a set of 600 proteins representative of the PDB native structures, we will then reanalyse the packing angle distribution after its proper rescaling with the newly

found reference distribution.

## Methods

### Databank and helix pair selection

We employed the same ensemble of 600 proteins considered by Chang et. al [9], which consisted of sequences varying in length from 44 to 1017, with low sequence homology and covering many different three-dimensional folds according to the Structural Classification of Proteins (SCOP) scheme [10]. The structures were monomeric and determined using x-ray crystallography. We collected 4397 helices each with at least four consecutive residues classified as helical in the PDB files. The average number of residues of these helices was 11.5. Two helices were defined to be in close contact, if at least one interhelical contact between  $C^\alpha$  atoms was present, with a maximal threshold distance of  $5.5\text{\AA}$  (analogous to condition  $C1$  in the text). Only helix pairs separated in sequence by at least 40 intervening residues were considered, to get rid of possible correlations induced by short loops. The resulting data set consisted of 1460 closely packed helix pairs.

### Helix axis reconstruction

The reconstruction of the helix axis from the coordinates of the  $C^\alpha$  atoms of the corresponding residues is a critical step in the determination of packing angle prefer-

ences. Since real helices can be bent, we adopted the procedure described by Walther *et al.* in ref. [6], in which a local axis is associated to every consecutive residue pair along the helix. The overall axis is thus a broken line consisting of short segments.

A good starting approximation for the local axis  $\mathbf{a}_i$ , based on the the four  $C^\alpha$  atom positions  $\mathbf{r}_{i-1}$ ,  $\mathbf{r}_i$ ,  $\mathbf{r}_{i+1}$ ,  $\mathbf{r}_{i+2}$ , was introduced by Chothia *et al.* [4]. We employed a slightly modified definition, where we first define the normalized bond vectors  $\mathbf{b}_i = (\mathbf{r}_{i+1} - \mathbf{r}_i) / |\mathbf{r}_{i+1} - \mathbf{r}_i|$ . In this way, the set of three orthonormal vectors  $\mathbf{t}_i$ ,  $\mathbf{v}_i$ ,  $\mathbf{u}_i$ , the natural reference system associated with the  $C^\alpha$  atom trace, can be defined without the distortions due to the fluctuations of the bond length between consecutive  $C^\alpha$  atoms in the following way [11]:  $\mathbf{t}_i = (\mathbf{b}_i + \mathbf{b}_{i-1}) / |\mathbf{b}_i + \mathbf{b}_{i-1}|$ ,  $\mathbf{v}_i = \mathbf{b}_i \times \mathbf{b}_{i-1} / |\mathbf{b}_i \times \mathbf{b}_{i-1}|$ ,  $\mathbf{u}_i = \mathbf{t}_i \times \mathbf{v}_i$ . If the  $C^\alpha$  atom trace followed a perfect ideal helix, the vector  $\mathbf{a}_i = \mathbf{u}_i \times \mathbf{u}_{i+1}$  would be parallel to the helix axis. We then initially determined the local axis between residues  $i$ ,  $i + 1$ , as the vector parallel to  $\mathbf{a}_i$ , of length  $1.45\text{\AA}$ , which has the geometric centre of the closest four consecutive  $C^\alpha$  atom positions,  $\mathbf{r}_{i-1}$ ,  $\mathbf{r}_i$ ,  $\mathbf{r}_{i+1}$ ,  $\mathbf{r}_{i+2}$ , as its midpoint. The two local axes at the helix termini were obtained by simply prolonging the neighbouring ones.

We then applied a smoothing procedure similarly to Walther *et al.* [6]. The ‘new’ local axes  $\mathbf{a}_i$  were obtained by averaging the direction of the closest three ‘old’ ones,  $\mathbf{a}_{i-1}$ ,  $\mathbf{a}_i$ ,  $\mathbf{a}_{i+1}$ , while conserving its midpoints. For the two local axes at the helix termini we averaged over the direction of the closest two available ones. To ensure the continuity of the overall axis, the inner hinges of the broken axial line were computed



as the midpoints between extremities of consecutive local vectors obtained from the running average. After repeating the whole procedure twice, the standard deviation of the distances of each  $C^\alpha$  atom from the reconstructed helix axis was  $0.16\text{\AA}$ .

The interaxial packing angle between two helices was computed between the local axis pair for which the minimum distance of closest approach was achieved. In case the segment of closest approach (SCA) intersected an inner hinge of the broken global axis, the local axis direction was defined as the average of the two corresponding local vectors. The whole discussion concerning the perpendicularity of both local axis direction with the SCA applies only to cases involving a terminal local axis, since face-to-face packing is anyway ensured in case of contact between inner local axes. Packing angles are positive if the background helix is rotated clockwise with respect to the frontal helix when facing them. The angle  $\Omega = 0^\circ$  ( $\Omega = \pm 180^\circ$ ) corresponds to parallel (antiparallel) helices with respect to their sequence direction.

Imposing the further requirement that the SCA intersected both local axis directions at a perpendicular angle within a threshold  $\tau_{\max}$  plays a critical role, as discussed in the text. For the three different  $\tau_{\max}$  values considered in this work,  $\tau_{\max} = 7^\circ, 11^\circ, 15^\circ$ , we collected datasets of 765, 837, 899 closely packed helix pairs, respectively.

As a final remark we report the mean value of the angle  $\Delta\Omega$  which is formed between consecutive local directions averaged over all inner hinges of all helical axes which were reconstructed using the procedure discussed above. We found  $\overline{\Delta\Omega} =$

$6.7^\circ \pm 4.0^\circ$ , strongly supporting the necessity of allowing a similar threshold when imposing angular constraints as in condition *C2*.

## Results and Discussion

### Geometrical analysis

We will now sketch the geometrical consequences of relaxing condition *C2* within a given threshold, in order to understand by means of a simple argument how this effects the random reference distribution. A comprehensive analytical treatment is in principle feasible but quite cumbersome. Numerical simulation will ultimately be the preferential approach to extract the corrected random reference distribution for interaxial angles.

Within the admitted threshold  $\tau_{\max}$ , cases similar to the one described in Fig. 1b may now occur. The SCA between the two helices, which intersects helix 1 at one of its axis ends and helix 2 at some internal point, forms an angle  $\theta_1$  which deviates from  $\frac{\pi}{2}$  by less than  $\tau_{\max}$ , whereas the GSCA does not intersect both helices (in this situation  $\tau_1 \neq 0, \tau_2 = 0$ ). If  $d < d_c$ , the two helices are considered to be in contact. The condition  $\tau_1 < \tau_{\max}$  is equivalent to the condition that GSCA intersects helix 1 within a distance  $\Delta l_{\max}$  from the end of its axis. This limit is reached when  $\theta_1 = \theta_{\min} \equiv \frac{\pi}{2} - \tau_{\max}$ .

There are also cases in which  $\tau_1 = 0$  and  $\tau_2 \neq 0$ , when the SCA intersects helix

2 at one of its axis ends and helix 1 at some internal point, and cases in which both  $\tau_1$  and  $\tau_2$  are not zero, and the SCA intersects both helices at one of their axes ends (Fig. 1c). In this last case, the geometrical condition implied by  $\tau_1 + \tau_2 < \tau_{\max}$ , and involving the distances  $\Delta l_1, \Delta l_2$  from the end of both helix axes to their intersection with the GSCA, is more complicated (and is discussed in the caption of Fig. 1).

Using the visual representation of Fig. 2b, we can say that allowing condition  $C2$  to be satisfied within the threshold  $\tau \equiv \tau_1 + \tau_2 < \tau_{\max}$ , opens up the possibility for the starting point of helix 2 to lie in the portion of space ( $\mathcal{G}$ ) formed by the four lightly shaded parallelograms (two parallel to helix 1 with sides  $h_1$  and  $\Delta \equiv \Delta l_{\max} \sin \Omega$ , and two parallel to helix 2 with sides  $h_2$  and  $\Delta$ ) and by the four remaining white corner regions ( whose boundaries are defined by hyperboles, see Figure 2 caption for details), which surround parallelogram  $A$ .

To compute the area of  $\mathcal{G}$  is not trivial, because of the hyperbole-shaped regions, but the result is obviously  $\Omega$  dependent. For example a simple trigonometric calculation shows that:

$$\Delta = \begin{cases} \frac{d \sin \tau_{\max}}{\sqrt{\sin^2 \Omega - \sin^2 \tau_{\max}}} & |\sin \Omega| > \sin \tau_{\max} \\ \infty & |\sin \Omega| \leq \sin \tau_{\max} \end{cases} \quad (2)$$

This implies that the area of  $\mathcal{G}$  diverges for  $|\sin \Omega| \leq \sin \tau_{\max}$ , which already points towards the fact that relevant corrections are possible even for small values of  $\tau_{\max}$ .

To conclude our analysis we need to enforce also condition  $C1$ . By using the pythagorean theorem it is easy to see that for any fixed  $d < d_c$ ,  $C1$  is satisfied for

any point (thought as starting point of helix 2) whose distance  $\Delta s(d_R) = \sqrt{d_R^2 - d^2}$  from parallelogram  $A$  is less than  $\Gamma = \Delta s(d_c) = \sqrt{d_c^2 - d^2}$ . These points belong to the region  $\mathcal{G}'$ , shown in Fig. 2c, formed by the 4 parallelograms (two of sides  $h_1$  and  $\Gamma$  and two of sides  $h_2$  and  $\Gamma$ ) and the four circular sectors (of radius  $\Gamma$ ) surrounding  $A$ . The area of  $\mathcal{G}'$  is independent on  $\Omega$  (see caption of Fig. 2c).

All the points in the portion of space  $\mathcal{H} = \mathcal{G} \cap \mathcal{G}'$  resulting from the intersection of  $\mathcal{G}$  and  $\mathcal{G}'$  satisfy both condition  $C1$  and  $C2$ .

Therefore, the probability  $P^{\tau_{\max}}(d)$  of selecting a particular angle  $\Omega$  with a tolerance  $\tau_{\max}$ , at a given distance  $d < d_c$ , is given by the product of the spherical polar term  $\sin \Omega$  [7] and a term proportional to the area of parallelogram  $A$  *plus* the area of  $\mathcal{H}$ .

When  $|\sin \Omega| < \sin \tau_{\max}$ , Eq.2 shows that  $\Delta$  diverges and thus:

$$P^{\tau_{\max}}(d) \sim \sin \Omega (h_1 h_2 \sin \Omega + 2(h_1 + h_2)\Gamma + B) \quad (3)$$

where  $B$  is the area of the corner regions in  $\mathcal{H}$ .

Since  $\Gamma$  does not depend on  $\Omega$ , the second term in the bracket will eventually dominate the small  $|\sin \Omega|$  behaviour of  $P^{\tau_{\max}}(d)$ . In practice, the actual relevance of this effect can be appreciated only after integrating  $P^{\tau_{\max}}(d)$  over  $d$ , since the relative weights of the different terms in the bracket vary with  $d$ . Such computation is quite cumbersome and we have rather chosen to get  $P^{\tau_{\max}}$  by simulating random helices which satisfy the contact conditions within a threshold  $\tau_{\max}$ , and to extract numerically the normalized histograms.

## Numerical simulations

In order to compute the reference distribution  $P^{\tau_{\max}}(\Omega)$  for interaxial packing angles we generated *random* helix pairs by means of computer simulations, and then selected them with the same conditions,  $C1$  and  $C2$ , used in extracting histograms from real helices in native protein structures. Note that when computing the reference distribution we did not take steric effects into account; in other words random helices might overlap.

More specifically, we constructed ideal discretized helices with the same geometrical properties of  $\alpha$ -helices in real proteins, i.e. twist per residue  $99.1^\circ$ , rise per residue  $1.45\text{\AA}$ , radius  $2.3\text{\AA}$  (as is the case when considering  $C_\alpha$  atoms). We chose to generate helices consisting of 11 residues, the average length in the dataset of real helices that we collected from the PDB. Keeping fixed the position of the first helix, the second helix was placed by firstly choosing randomly the midpoint of its axis within a sphere of radius  $15\text{\AA}$  centred in the midpoint of the first helix axis, and then selecting, again randomly, both the direction of its axis and the twist of its first residue.

Boundary effects might be relevant, when the radius of the sphere in which the second helix is generated is too small with respect to the helix length and helix finiteness is effectively reduced. We made sure that our results did not change when increasing the radius of the sphere in which the second helix axis is placed.

We generated  $5 \cdot 10^7$  random helix pairs, 29915472 out of which satisfied condition  $C1$  of having at least one pair of residues distant less than  $5.5\text{\AA}$ . Condition  $C2$  was

then applied, in the same way as explained in Methods for the real helices data set, with the whole axis being now a segment in the ideal case. In this way we generated 11467456, 13033815, 14553626 helix pairs, respectively, for the three different  $\tau_{\max}$  values considered in this work,  $\tau_{\max} = 7^\circ, 11^\circ, 15^\circ$ .

In Fig. 3 we plot the corresponding random reference distributions  $P^{\tau_{\max}}(\Omega)$ , comparing them with the ideal ( $\tau_{\max} = 0$ ) case:  $P(\Omega) \sim \sin^2 \Omega$ . The difference, although due to a very subtle effect is substantial, and it is clearly seen that a new regime is present for  $|\sin \Omega| < \sin \tau_{\max}$ , as expected from the previous discussion.

## Reanalysing experimental results

To test the effect of this new reference distribution we have recomputed an experimental distribution of interaxial angles (see Methods for details) by analysing a databank of 600 proteins and using a contact threshold  $d_c = 5.5\text{\AA}$  and a tolerance  $\tau_{\max} = 7^\circ$ , corresponding the intrinsic uncertainty  $\overline{\Delta\Omega} = 6.7^\circ$  estimated when determining local axis directions (see Methods). The histogram is reported in the upper panel of Fig. 4: in order to obtain good statistics for each single bin, we gathered results every  $15^\circ$ . The histogram is consistent with previous analysis [6, 7, 8]. In the middle panel of Fig. 4 we plot  $P^{7^\circ}(\Omega)$  and, for reference,  $P(\Omega)$  normalized with the same binning as in the previous panel. Finally, in the lower panel of Fig. 4 we present the histogram both rescaled with  $P^{7^\circ}(\Omega)$  and with  $P(\Omega)$ . The results are clear and striking: the correct distribution  $P^{7^\circ}(\Omega)$  removes the spurious peaks at  $0^\circ$  and  $\pm 180^\circ$ , whereas 4

out of the 6 predicted packing angles [6] arise as clean local maxima in the expected positions. Only two of the predicted packing angles are clearly not favoured according to our analysis. Remarkably, the two peaks theoretically predicted at  $143.9^\circ$  and  $-158^\circ$ , that were seen as shoulders in the unrescaled histogram, are instead placed in the correct position (within binning uncertainty) in the rescaled histogram. We also note that a residual preference for parallel and antiparallel alignment of two contacting helices cannot be ruled out even after proper rescaling. Because of small statistics, it is difficult to ascertain whether this is a genuine effect or is just due to the tail superposition of different preferential angle peaks. In order to further test both the robustness of the results and the full procedure we have obtained statistical histograms from the experimental data using three different thresholds,  $\tau_{\max}$ . Since we can compare them with the corresponding random distribution we should expect three similar rescaled histograms. This is nicely confirmed by Fig. 5, where the three rescaled histograms show a very good overlap, within the statistical uncertainty. We also note that generally, the greater the threshold used to relax condition *C2*, the more blurred the peaks corresponding to the sterically preferred angles. This confirms that condition *C2* is needed to ensure face-to-face packing and the applicability of steric models.

## Conclusion

In this paper we have shown that the calculation of the probability distribution of interaxial angles between random finite helices which are in contact is not a trivial geometric problem, because of the approximations introduced to ensure face-to-face packing between contacting helices. Such approximations are unavoidable, due to the imperfect shape of natural occurring helices which do not have well defined axes. Although analytical results can be found to estimate the correct random distribution, the simplest way to obtain it consists in using numerical simulations. We have presented a re-analysis of the distribution of packing angles rescaled with our new reference distribution and we have found a remarkable agreement with the packing angles predicted by steric models [6].

## References

- [1] Crick, F.H.C. (1953) *Acta Crystallog.* **6**, 689-697.
- [2] Richmond, T.J., Richards, F.M. *J. Mol. Biol.* **119**, 537-555 (1978).
- [3] Chothia, C., Levitt, M., Richardson, D. (1977) *Proc. Natl. Acad. Sci. USA* **74**, 4130-4134.
- [4] Chothia, C., Levitt, M. Richardson, D. (1981) *J. Mol. Biol.* **145**, 215-250.
- [5] Efimov, A.V. (1979) *J. Mol. Biol.* **134**, 23-40.



- [6] Walther, D., Eisenhaber, F., Argos, P. (1996) *J. Mol. Biol.* **255**, 536-553.
- [7] Bowie, J.U. (1997) *Nature Struct. Biol.* **4**, 915-917.
- [8] Walther, D., Springer, C., Cohen, F.E. (1998) *Proteins: Struct. Funct. Genet.* **33**, 457-459.
- [9] Chang, I., Cieplak, M. , Dima, R.I., Maritan, A., Banavar, J.R. (2001) *Proc. Natl. Acad. Sci. USA* **98**, 14350-14355.
- [10] Murzin, A.G. , Brenner, S.E., Hubbard, T., Chothia, C. (1995) *J. Mol. Biol.* **247**, 536-540.
- [11] Rey, A., Skolnick, J. *J. Comput. Chem.* **13**, 443-456 (1992).

## Acknowledgments

We are indebted to Amos Maritan for stimulating discussions and advice, Giuseppe Zanotti for helpful suggestions and Iksoo Chang for his invaluable help in providing us with the protein databank used in ref. [9]. We thank Harvey Dobbs for a critical reading of the manuscript. This work was supported by INFM, MIUR COFIN-2001 and FISR 2002.

# Figure Legends

## Figure 1

a) The global segment of closest approach (GSCA), of length  $d$ , between two straight lines is, by definition, perpendicular to both of them. The segment of closest approach (SCA), of length  $d_r$ , between two helices (schematically represented by cylinders) surely coincides with the global one if it intersects both helices within their axis length. This fact is always guaranteed if the two helices are assumed to have infinite length (hypothesis of Ref. [7]).

b) The two finite helices have a SCA that is not coincident with the GCSA. The latter intersects helix 1 at a distance  $\Delta l_1$  from its end and may (as in the picture) or may not intersect helix 2. The former joins the end point of helix 1 to a point inside helix 2. The angle formed with helix 1 ( $\theta_1$ ) is deviating from  $\pi/2$  by an amount  $\tau_1$ . Instead  $\theta_2 = \frac{\pi}{2}$  and  $\tau_2 = 0$ . The trigonometric relation expressing  $\Delta l_1$  as an increasing function of  $\tau_1$  can be easily obtained:  $\Delta l_1(\tau) = \frac{d \sin \tau_1}{\sin \Omega \sqrt{\sin^2 \Omega - \sin^2 \tau_1}}$ . When  $\tau_1 < \tau_{\max}$ , condition C2, defined in the text, is still fulfilled. This is equivalent to require that  $\Delta l_1 \leq \Delta l_{\max} \equiv \Delta l_1(\tau_{\max})$ . Notice that  $\Delta l_1(\tau_1)$  diverges when  $\tau_1$  approaches  $\Omega$  from below, and consequently, when  $|\sin \Omega| < \sin \tau_{\max}$ ,  $\Delta l_{\max}$  diverges. In such regime the condition C2 (but obviously not C1 because  $d_r$  may also diverge) is always satisfied within the allowed tolerance. A similar situation and a similar analysis can be done for  $\tau_1 = 0$  and  $\tau_2 \neq 0$ .

c) GSCA is neither intersecting helix 1 nor helix 2 and the SCA is joining two endpoints. In the case depicted in the figure the two helices are placed in opposite sides with respect to the GSCA. The threshold condition  $\tau_1 + \tau_2 < \tau_{\max}$  may be translated into the following one involving  $\Delta l_1$  and  $\Delta l_2$ :  $((\Delta l_1 + \Delta l_2 \cos \Omega)(\Delta l_2 + \Delta l_1 \cos \Omega) - \sqrt{(d^2 + \Delta l_1^2 \sin^2 \Omega)(d^2 + \Delta l_2^2 \sin^2 \Omega)}) / ((\Delta l_1 + \Delta l_2 \cos \Omega)\sqrt{d^2 + \Delta l_1^2 \sin^2 \Omega} + (\Delta l_2 + \Delta l_1 \cos \Omega)\sqrt{d^2 + \Delta l_2^2 \sin^2 \Omega}) > \cot \tau_{\max}$ . Situations in which the two helices are placed on the same side with respect to the GSCA are also possible. In this case the condition becomes  $((\Delta l_1 - \Delta l_2 \cos \Omega)(\Delta l_2 - \Delta l_1 \cos \Omega) - \sqrt{(d^2 + \Delta l_1^2 \sin^2 \Omega)(d^2 + \Delta l_2^2 \sin^2 \Omega)}) / ((\Delta l_1 - \Delta l_2 \cos \Omega)\sqrt{d^2 + \Delta l_1^2 \sin^2 \Omega} + (\Delta l_2 - \Delta l_1 \cos \Omega)\sqrt{d^2 + \Delta l_2^2 \sin^2 \Omega}) > \cot \tau_{\max}$ .

## Figure 2

a) In this figure, the position of helix 1 (represented by a vector of length  $h_1$ ) and a vector orthogonal to the paper plane, determining the direction of the GSCA to a second helix, are fixed. Given a particular packing angle  $\Omega$ , in order to satisfy condition C2 without any tolerance  $\tau_{\max}$ , a second finite helix axis (of length  $h_2$ ) may then be placed only within a plane parallel to the paper plane and such that its starting point is inside the dark shaded parallelogram  $A$ . Otherwise the SCA between the two finite axes would no longer be perpendicular to both of them. The area of parallelogram  $A$  is  $h_1 h_2 \sin(\Omega)$ .

b) The tolerance  $\tau_{\max}$  with which the condition of perpendicularity between the SCA and the two helices is implemented enlarges the portion of space where the

starting point of helix 2 can be placed. The region  $\mathcal{G}$  formed by the four lightly shaded parallelograms and the four white corner regions, which together surround parallelogram  $A$ , can now be exploited. The two parallelograms parallel to helix 2, whose sides are  $h_2$  and  $\Delta = \Delta_{\max} \sin \Omega$ , are due to the geometric arrangement described in Fig. 1b with  $\tau_1 \neq 0$  and  $\tau_2 = 0$  (the vector with the dashed starting point represent the possible location of helix 2 in such context). The two other parallelograms, parallel to helix 1, with sides  $h_1$  and  $\Delta$ , correspond to the similar case  $\tau_1 = 0$  and  $\tau_2 \neq 0$ . The four remaining white regions, corresponding to the case  $\tau_1 \neq 0$  and  $\tau_2 \neq 0$ , are all limited by hyperbola-like curves. The two of them subtending an obtuse angle are due to the geometric arrangement described in Fig. 1c, corresponding to the two helices being placed in opposite sides with respect to the GSCA (the vector with the white starting point represent the possible location of helix 2 in such context). The two of them subtending an acute angle correspond to the two helices being placed in the same side with respect to the GSCA. In both cases it is possible to find the equation describing such boundary curves, which we omit here for the sake of simplicity. The area of  $\mathcal{G}$  is  $2(h_1 + h_2)\Delta$  plus a non trivial contribution coming from the four corner regions.

c) The distance constraint C1 limits by itself the portion of plane surrounding parallelogram  $A$  where the starting point of the second helix can be placed. This region  $\mathcal{G}'$  is simply the locus of points whose Euclidean distance from  $A$  in the paper plane is less than  $\Gamma \equiv \sqrt{d_c^2 - d^2}$ . For given values of  $d$  and the distance threshold  $d_c$ ,

this region is thus formed by the four lightly shaded parallelograms and by the four white circular sectors. The area of  $\mathcal{G}'$  is  $2(h_1 + h_2)\Gamma + \pi\Gamma^2$ .

### Figure 3

Ideal ‘random’ distribution of interaxial packing angles for four different values of the angle threshold  $\tau_{\max}$  used in applying condition *C2*;  $\tau_{\max} = 0^\circ$  (upper left panel),  $\tau_{\max} = 7^\circ$  (upper right panel),  $\tau_{\max} = 11^\circ$  (lower left panel),  $\tau_{\max} = 15^\circ$  (lower right panel). The four distributions were computed by means of numerical simulations described in Methods. Since ideal helices do not have a preferential order, the histograms show in this figure have been restricted to the  $-90^\circ < \Omega < 90^\circ$  region. The 14553626 packing angle values collected in the  $\tau_{\max} = 15^\circ$  histogram were then successively filtered out by the more and more restrictive  $\tau_{\max} = 11^\circ$ ,  $\tau_{\max} = 7^\circ$ ,  $\tau_{\max} = 0^\circ$  threshold conditions to generate the 13033815, 11467456, 8646994 data, respectively, collected in the corresponding histograms. The dashed line is the fit of the  $\tau_{\max} = 0^\circ$  data, obtained enforcing condition *C2* in a strict way, to the expected  $P(\Omega) \sim \sin^2 \Omega$  distribution, which is then reported for comparison in all other histograms. All histograms were constructed with a bin width of  $1.5^\circ$ . Histograms are normalized in such a way that a flat distribution would correspond to a constant 1 height.

## Figure 4

Upper Panel. Experimental ‘bare’ unrescaled distribution of interaxial packing angles between contacting helices. Data were obtained with a distance threshold  $d = 5.5\text{\AA}$  for interhelical  $C_\alpha$  atom pairs and an angular threshold  $\tau_{\max} = 7^\circ$  for condition C2. The histogram is normalized in such a way that a flat distribution would correspond to a constant 1 height.

Middle Panel. Ideal ‘random’ distribution which have to be used to rescale the ‘bare’ experimental distribution, in order to reveal true packing angle preferences. The two different distributions obtained with either  $\tau_{\max} = 0^\circ$  (thick line) or  $\tau_{\max} = 7^\circ$  (filled columns) are shown. Histograms are normalized in such a way that a flat distribution would correspond to a constant 1 height.

Lower Panel. Rescaled distribution of interaxial packing angles. The experimental ‘bare’ distribution in the upper panel is divided by the ideal ‘random’ one in the middle panel, obtained with either  $\tau_{\max} = 0^\circ$  (blue line) or  $\tau_{\max} = 7^\circ$  (filled columns). Histogram heights greater than 1 correspond to preferential packing angles, whereas heights lower than 1 correspond to disfavoured packing angles.

All histograms were constructed with a bin width of  $15^\circ$ . Arrows in the upper and lower panels mark the values of the six preferred packing angles predicted by Walther *et al.* [6];  $\Omega_{\text{abc}} = -37.1^\circ, -97.4^\circ, 22.0^\circ$ , each represented twice with a periodicity of  $180^\circ$ .

## Figure 5

Rescaled distribution of interaxial packing angles between contacting helices for three different values of the angle threshold  $\tau_{\max}$  used in enforcing condition  $C2$ ;  $\tau_{\max} = 7^\circ$  (light grey filled columns),  $\tau_{\max} = 11^\circ$  (dark grey line),  $\tau_{\max} = 15^\circ$  (black line). Each histogram was obtained by dividing the experimental unrescaled distribution by the corresponding ideal reference one (we used the three distributions represented in Fig. 3 with a different binning). All histograms were constructed with a bin width of  $15^\circ$ . Note that the histograms are not normalized, being computed as the ratio of two normalized histograms. The arrows mark the values of the the six optimal packing angles predicted by Walther *et al.* [6].

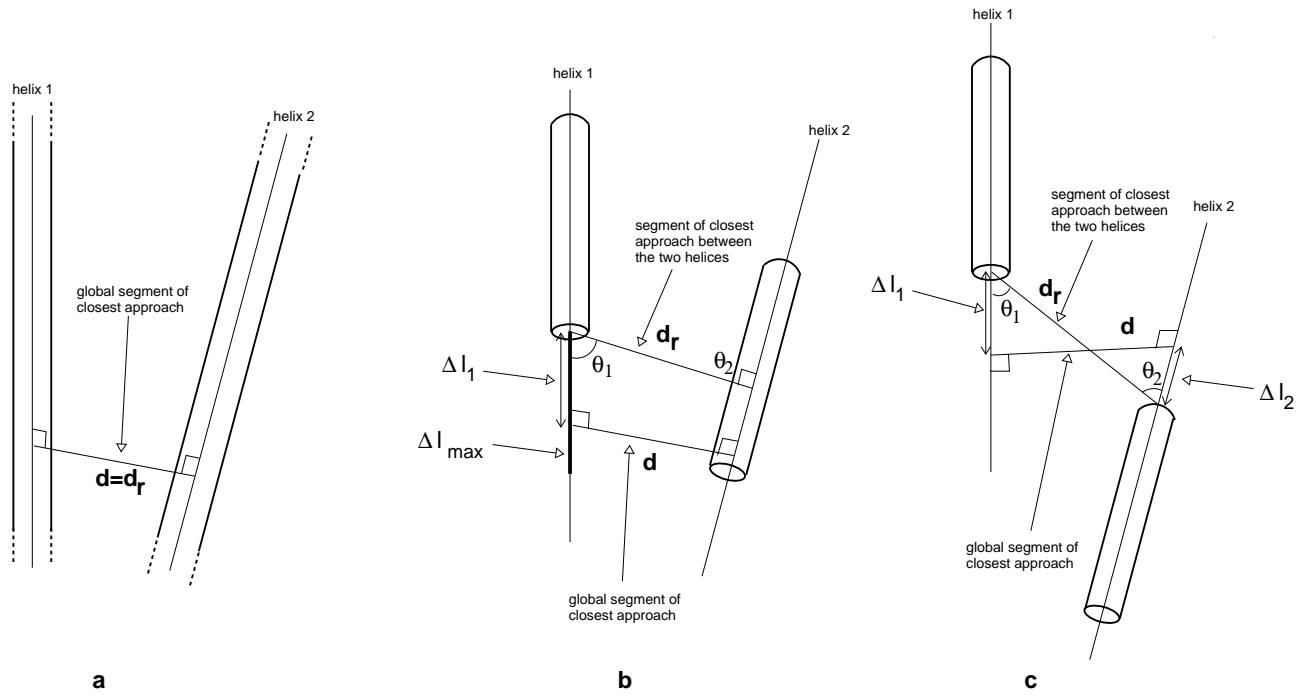
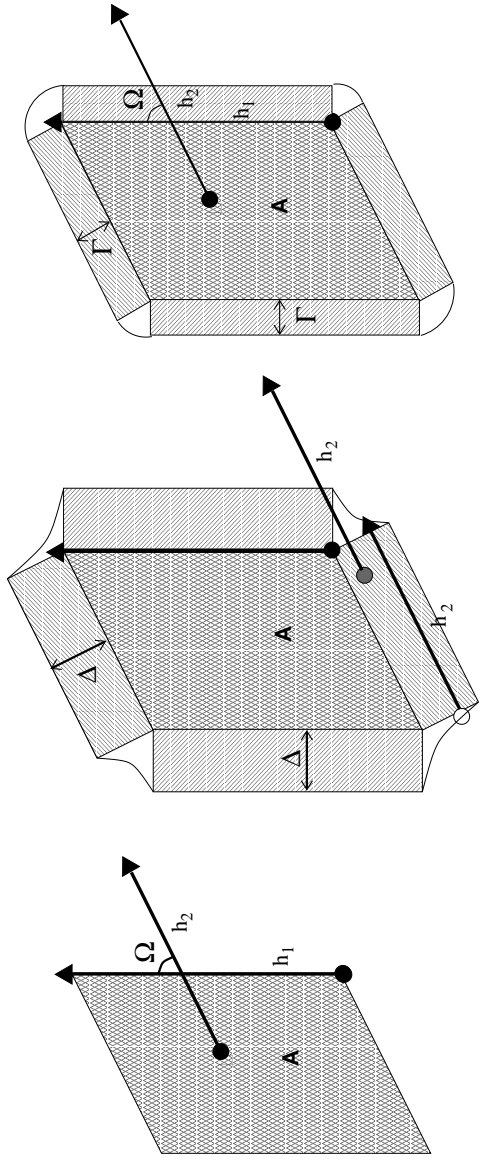


Figure 1





**a**

**b**

**c**

**Figure 2**

Random reference distribution

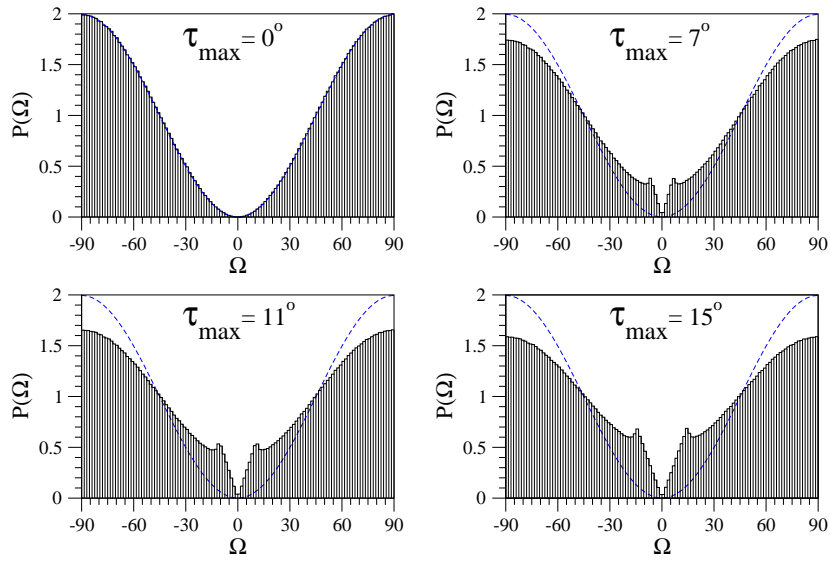


Figure 3

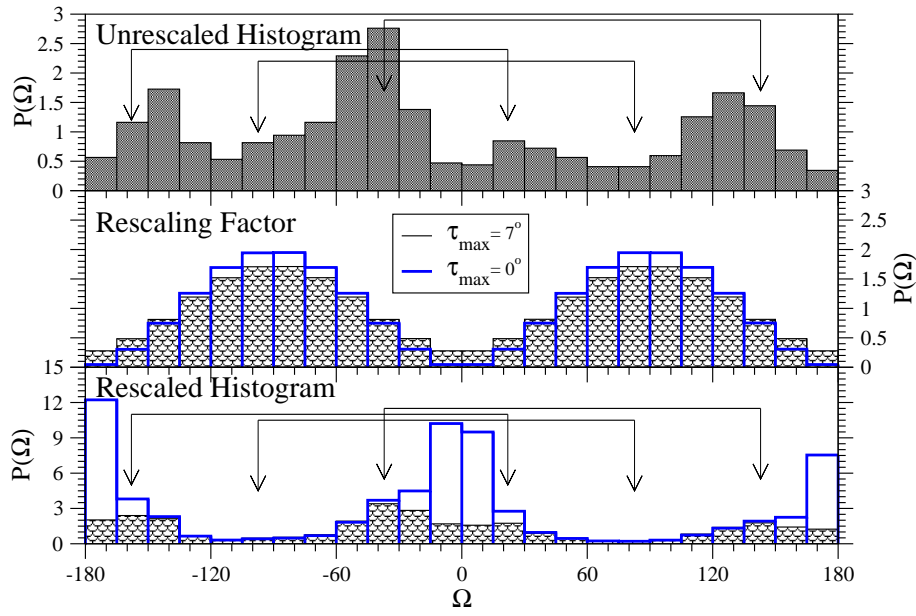


Figure 4

Rescaled Packing Angle Histograms

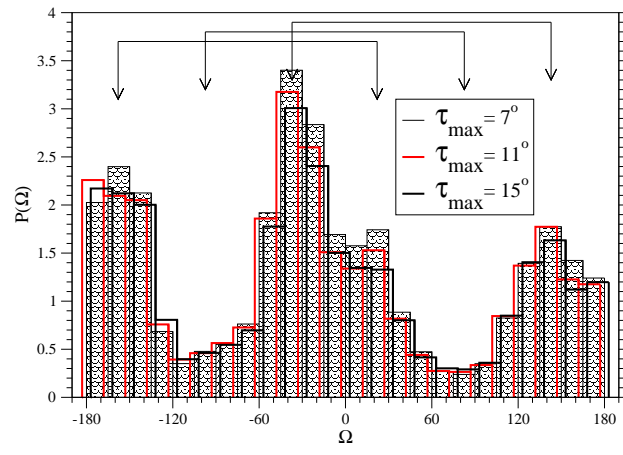


Figure 5